Current-driven second-harmonic domain wall resonance in ferromagnetic metal/nonmagnetic metal bilayers: A field-free method for spin Hall angle measurements

M. R. Hajiali,[1] M. Hamdi,[2] S. E. Roozmeh,[1] and S. M. Mohseni[2,*]
[1]*Department of Physics, University of Kashan, 87317 Kashan, Iran*
[2]*Faculty of Physics, Shahid Beheshti University, Evin, 19839 Tehran, Iran*
(Received 4 May 2017; revised manuscript received 24 July 2017; published 5 October 2017)

We study the ac current-driven domain wall motion in bilayer ferromagnetic metal (FM)/nonmagnetic metal (NM) nanowires. The solution of the modified Landau-Lifshitz-Gilbert equation including all the spin transfer torques is used to describe motion of the domain wall in the presence of the spin Hall effect. We show that the domain wall center has a second-harmonic frequency response in addition to the known first-harmonic excitation. In contrast to the experimentally observed second-harmonic response in harmonic Hall measurements of spin-orbit torque in magnetic thin films, this second-harmonic response directly originates from spin-orbit torque driven domain wall dynamics. Based on the spin current generated by domain wall dynamics, the longitudinal spin motive force generated voltage across the length of the nanowire is determined. The second-harmonic response introduces additionally a practical field-free and all-electrical method to probe the effective spin Hall angle for FM/NM bilayer structures that could be applied in experiments. Our results also demonstrate the capability of utilizing FM/NM bilayer structures in domain wall based spin-torque signal generators and resonators.

DOI: 10.1103/PhysRevB.96.144406

I. INTRODUCTION

Current-induced domain wall (DW) dynamics in magnetic nanostructures raised great research interest in the field of spintronics because of its prospective applications in novel devices including DW-based shift register [1], logic [2], racetrack memory [3], and DW collision spin wave emitters [4]. Current-induced DW motion (CIDWM) in magnetic nanowires can occur thanks to the spin transfer torque (STT) effect due to exchange coupling between local magnetization of DWs and spin-polarized currents [5–9]. There are two types of STTs acting on a noncollinear magnetization texture, e.g., a DW, when a spin-polarized current flows through it, namely, adiabatic and nonadiabatic terms. It has been shown theoretically [5,10] that the initial DW velocity is mostly controlled by the adiabatic term, while the nonadiabatic term is responsible for its terminal velocity.

In ferromagnetic metal/nonmagnetic metal (FM/NM) bilayers, a spin current generated by the spin Hall effect (SHE) through the adjacent NM layer can be injected into the FM layer [11] that produces another type of STT, named spin-orbit torque (SOT), which can result in magnetization dynamics and CIDWM [12–16]. For instance, SOT can significantly reduce the critical dc current density to depinning a DW from a pinning potential, therefore causing lowering of the energy consumption for operation of DW-based electronic devices [17].

Investigations of the dynamical response of DW to ac currents have resulted in many achievements including determination of the mass of DW [18,19], micrometer range DW displacement [18,19], and resonant control of DW movement [20–22]. Furthermore, depinning of a DW benefits more from the ac current than from the dc current because of current-induced DW resonance [23]. Therefore, to benefit from such a dynamically rich feature, uncovering the dynamics of DWs under ac current and SOT is important and remains unclear.

Since the discovery of SHE in semiconductors [24,25] and metals [26,27], various techniques have been developed to determine the conversion rate of charge currents to spin currents, named the spin Hall angle, θ_{SH}. All these methods including cavity ferromagnetic resonance (C-FMR) spectrometry [28,29], spin pumping (SP) [30], spin-torque FMR (ST-FMR) [31,32], hybrid phase-resolved optical-electrical FMR (OE-FMR) [33], and determining the DW velocity using magneto-optical microscopy [34,35] require almost strong bias magnetic fields to saturate the FM layer or in some cases a complicated measurement setup. Hence, a field-free measurement technique of θ_{SH} is a challenge.

In this paper, we investigate the ac CIDWM in FM/NM bilayers (Fig. 1) based on a collective coordinate approach. The FM layer has perpendicular magnetic anisotropy and the NM layer has a strong spin-orbit interaction responsible for the SHE. All current-induced STTs and the SOT are included in our study. By solving equations of DW motion, we obtained second-harmonic motion in addition to the known first-harmonic motion. This second-harmonic response has a different nature in comparison with that observed in the second-harmonic Hall measurements of SOT [36–41] in single domain FM/NM structures. The former, which we study here, originates from SOT exerted on a DW due to the ac SHE occurring in the NM layer, while the latter originates from anomalous Hall and spin Hall magnetoresistance effects [36–41].

Finally, we calculated the spin motive force (SMF) voltage induced by DW motion. Our results propose a field-free method to measure the effective spin Hall angle for such bilayer structures. In addition, second-harmonic DW motion in the presence of SHE and ac current can further be used in recently reported DW and skyrmion based high-frequency signal generators and resonators [20,21,42] to obtain higher frequencies.

*Corresponding author: m-mohseni@sbu.ac.ir; majidmohseni@gmail.com.

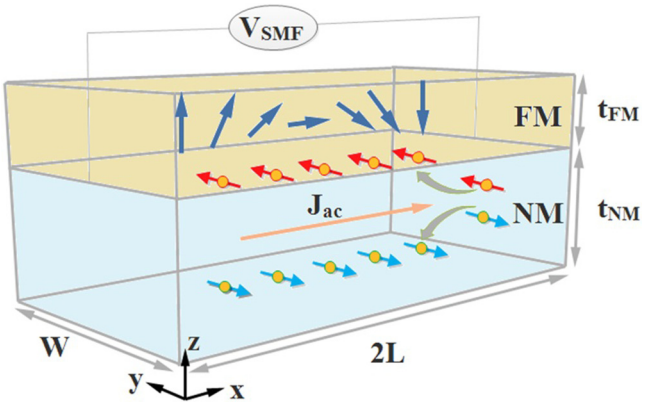

FIG. 1. Schematic illustration of a FM/NM bilayer system. An in-plane ac current density J_{ac} generates a perpendicular spin current, which exerts SOT on FM.

II. MODEL

A. ac current-induced domain wall motion in presence of spin Hall effect

We considered a bilayer strip wire with dimensions $2L \times w \times (t_F + t_N)$ along x, y, and z directions, where $2L$ is the length and w is the width of the bilayer wire, t_F and t_N represent the thickness of the FM and NM layers, respectively, and $L \gg w$, t_F,t_N. An in-plane ac current applied along the x direction generates conventional adiabatic and nonadiabatic STTs and SOT acting on a DW within the FM. The geometry of the structure is shown in Fig. 1. The modified Landau-Lifshitz-Gilbert (LLG) equation including all the STTs is given by

$$\frac{\partial \mathbf{m}}{\partial t} = -\gamma \mathbf{m} \times \mathbf{H}_{\text{eff}} + \alpha \mathbf{m} \times \frac{\partial \mathbf{m}}{\partial t} - a_J \mathbf{m} \times \left(\mathbf{m} \times \frac{\partial \mathbf{m}}{\partial t} \right) - n_J \mathbf{m} \times \frac{\partial \mathbf{m}}{\partial x} - \theta_{\text{SH}} c_J \mathbf{m} \times (\mathbf{m} \times \hat{y}), \quad (1)$$

where $\mathbf{m}$ is the unit vector along the magnetization direction, γ is the gyromagnetic ratio, $\mathbf{H}_{\text{eff}}$ is effective field including the exchange, anisotropy, and external fields, α is the Gilbert damping constant, $a_J = (\hbar \gamma P / 2eM_s) J_F$ is the magnitude of adiabatic STT in velocity dimension, $n_J = \beta a_J$ is the magnitude of nonadiabatic STT and β is the nonadiabaticity coefficient, $\theta_{\text{SH}} c_J = (\theta_{\text{SH}} \hbar \gamma J_N / 2eM_s t_F)$ is the magnitude of SOT, where θ_{SH} is an effective spin Hall angle for the bilayer system, $\hbar$ is the reduced Planck constant, P is the spin polarization in FM, e is electron charge, M_s is the saturation magnetization of FM, and J_F (J_N) is applied current density in FM (NM). J_F and J_N are determined by Ohm's law for two parallel resistors as $J_F = J(\frac{\sigma_F}{\sigma_F + \sigma_N})$ and $J_N = J(\frac{\sigma_N}{\sigma_F + \sigma_N})$, where J is the average current density in a bilayer nanowire and σ_F (σ_N) is the conductivity of FM (NM).

Introducing the magnetization direction as $\boldsymbol{m} = (\sin\theta \cos\varphi, \sin\theta \sin\varphi, \cos\theta)$, the micromagnetic energy density u in polar coordinates θ and φ is given by

$$u = A_{\text{ex}} \left[\left(\frac{\partial \theta}{\partial x} \right)^2 + \left(\sin\theta \frac{\partial \varphi}{\partial x} \right)^2 \right] + K_u \sin^2\theta + K_d \sin^2\theta \sin^2\varphi, \quad (2)$$

where A_{ex} is the exchange stiffness coefficient and K_u and K_d are perpendicular and in-plane anisotropy constants, respectively. A dynamic DW structure is considered as $\theta(x,t) = 2\arctan[\exp(\frac{x-q(t)}{\Delta(t)})]$ and $\varphi(x, t) = \phi(t)$, where $q(t)$ and $\Delta(t)$ represent the DW center position and width, respectively [43]. The chirality of the DW is determined by angle $\phi(t)$ and distortion of the wall width is small during wall motion, hence we suppose $\Delta(t) \cong \sqrt{A/K_u}$. The restoring energy density arising from geometric notch [20,44], impurity or demagnetization field [23] induced pinning is assumed to be of the form $u_r = k\, q^2/2$. Therefore, equations of motion for two collective coordinates q and ϕ in rigid DW limit, by neglecting the small coefficients of nonlinear terms, are given by

$$m \frac{\partial^2 q}{\partial t^2} + b \frac{\partial q}{\partial t} + kq = -\frac{2M_S}{\gamma} \left(\frac{n_J}{\Delta} + \frac{1}{\gamma \Delta H_d} \times \left(\alpha \frac{\partial n_J}{\partial t} + \frac{\partial a_J}{\partial t} \right) + \frac{\alpha a_J n_J B_{\text{SH}}}{\gamma \Delta^2 H_d} \right), \quad (3)$$

$$m \frac{\partial^2 \phi}{\partial t^2} + b \frac{\partial \phi}{\partial t} + k\phi = \frac{k a_J}{\gamma \Delta H_d} + \frac{2M_S \alpha}{\Delta^2 \gamma^2 H_d} \frac{\partial a_J}{\partial t} - \frac{2M_S}{\Delta^2 \gamma^2 H_d} \frac{\partial n_J}{\partial t}, \quad (4)$$

where $H_d = (2K_d/M_s) = 4\pi M_s$ is the demagnetization field, $B_{\text{SH}} = \theta_{\text{SH}} c_J (\pi \Delta e M_s / P J_F \hbar \gamma) = (\pi \theta_{\text{SH}} \Delta J_N / 2 t_F P J_F)$, $m = (1+\alpha^2) \frac{2M_s}{\gamma^2 \Delta H_d}$, and $b = \alpha(\frac{2M_s}{\gamma \Delta} + \frac{k}{\gamma H_d})$.

Considering an ac applied current with frequency ω, Eq. (3) describes forced damped oscillations. Therefore, the steady-state solution to q is of the form

$$\begin{aligned} q(t) &= q_{1\omega}(t) + q_{2\omega}(t), \\ q_{1\omega}(t) &= A_\omega \cos[\omega t - (\delta - \rho)], \\ q_{2\omega}(t) &= A_{2\omega} \cos[2\omega t - \xi], \end{aligned} \quad (5)$$

where $q_{1\omega}(t)$, $q_{2\omega}(t)$ are the first- and second-harmonic components of DW motion. A_ω and $A_{2\omega}$ are the first- and second-harmonic DW motion amplitudes, respectively, and are given by

$$A_\omega = -\frac{2M_S}{\gamma} \left(\frac{\sqrt{\frac{n^2}{\Delta^2} + \frac{(\alpha n + a)^2 \omega^2}{(4\pi\gamma \Delta M_S)^2}} \left(\frac{\sigma_F}{\sigma_F + \sigma_N} \right) J}{\sqrt{(k - m\omega^2)^2 + \omega^2 b^2}} \right), \quad (6)$$

$$A_{2\omega} = -\frac{2M_S}{\gamma} \left(\frac{\frac{\alpha n a B_{\text{SH}}}{4\pi\gamma\Delta^2 M_S} \left(\frac{\sigma_F}{\sigma_F + \sigma_N} \right)^2 J^2}{\sqrt{(k - 4m\omega^2)^2 + 4\omega^2 b^2}} \right). \quad (7)$$

$\phi(t)$ has no second-harmonic dynamics and is obtained as

$$\phi(t) = \phi_\omega \cos[\omega t - (\delta + \eta)], \quad (8)$$

where the chirality amplitude is

$$\phi_\omega = \frac{2M_S}{\gamma} \left(\frac{\sqrt{\left(\frac{ak}{8\pi \Delta M_S^2} \right)^2 + \frac{(n - \alpha a)^2 \omega^2}{(4\pi\gamma\Delta^2 M_S)^2}} \left(\frac{\sigma_F}{\sigma_F + \sigma_N} \right) J}{\sqrt{(k - m\omega^2)^2 + \omega^2 b^2}} \right). \quad (9)$$

The phases δ, ρ, ξ, and η are in the form of

$$\begin{aligned}\delta &= \arctan\left[b\omega/(k-m\omega^2)\right],\\ \rho &= \arctan\left[(\alpha n+a)\omega/(4\pi M_S\gamma n)\right],\\ \xi &= \arctan\left[2b\omega/(k-4m\omega^2)\right],\\ \eta &= \arctan\left[2M_S\omega(n-\alpha a)/\Delta\gamma ak\right].\end{aligned} \tag{10}$$

According to Eqs. (6), (7), and (9) the first-harmonic DW motion amplitude A_ω and chirality amplitude ϕ_ω are proportional to the applied current density J, while the second-harmonic amplitude is proportional to the J^2 due to ac SOT.

B. Spin currents and voltages

A given dynamical noncollinear magnetization texture, $\mathbf{m}(r,t)$, generates a spin current which is given by [45–48]

$$J_i^s = \frac{\mu_B\hbar}{2e^2}\sum_k \sigma_{ik}^c\left[\left(\frac{\partial\mathbf{m}}{\partial t}\times\frac{\partial\mathbf{m}}{\partial r_k}\right)\cdot\mathbf{m} + \beta\frac{\partial\mathbf{m}}{\partial t}\cdot\frac{\partial\mathbf{m}}{\partial r_k}\right], \tag{11}$$

where J_i^s is the ith component of spin current, $\boldsymbol{J}^s = (J_x^s, J_y^s, J_z^s)$, which flows through the i direction ($i,j,k = x,y,z$) and its polarization is determined by the instantaneous local magnetization direction, $\mathbf{m}(r,t)$, σ_{ik}^c is the ik-element of the electrical conductivity tensor of FM, $r_k = x$, y, z, and μ_B is the Bohr magneton. All other parameters are previously determined. Such spin current generates electrical currents or voltages in FM/NM bilayers through two dominant mechanisms: (i) spin motive force (SMF) within the FM layer and (ii) inverse spin Hall effect (ISHE) within the NM layer. SMF is related to the s-d exchange coupling between conduction electrons and localized moments within FM; whereas, ISHE is the reciprocal effect of SHE, i.e., an injected spin current into NM is converted to a transverse electrical current or voltage. In the case of our study and considering the dynamic DW structure introduced earlier, the only nonvanishing spatial derivative of magnetization is $\partial\mathbf{m}(r,t)/\partial x$. Furthermore, most of the common FMs have a cubic or hexagonal crystal structure and hence their conductivity tensor is diagonal. Therefore, according to Eq. (9), all components of spin current vanish except J_x^s and $\boldsymbol{J}^s = (J_x^s, 0, 0)$. As the z-direction flowing component of the spin current, $J_z^s = 0$, no spin current enters the NM layer, hence no charge current or voltage is generated through ISHE. The local current density generated by the SMF mechanism is given by

$$J_{i,\mathrm{SMF}}^c = \frac{eP}{\mu_B}J_i^s. \tag{12}$$

Here, $J_{i,\mathrm{SMF}}^c$ is the charge current density flowing through the i direction generated by SMF. Using Eqs. (9) and (10) and a dynamic DW structure with $\partial\theta/\partial t = -(\partial\theta/\partial x)(\partial q/\partial t)$ and $\partial\theta/\partial x = (\sin\theta/\Delta)$, one can obtain the charge current density induced by SMF in polar coordinates as

$$\begin{aligned}J_{x,\mathrm{SMF}}^c &= \frac{P\hbar\sigma_F}{2e}\left[-\frac{\partial\theta}{\partial x}\frac{\partial\varphi}{\partial t}\sin\theta+\beta\frac{\partial\theta}{\partial x}\frac{\partial\theta}{\partial t}\right]\\ &= -\frac{P\hbar\sigma_F}{2e}\left[\frac{1}{\Delta}\frac{\partial\phi}{\partial t}+\frac{\beta}{\Delta^2}\frac{\partial q}{\partial t}\right]\sin^2\theta.\end{aligned} \tag{13}$$

Averaging SMF charge current density over the wire length, $\langle J_{x,\mathrm{SMF}}^c\rangle = \frac{1}{2L}\int_{-L}^{L} J_{x,\mathrm{SMF}}^c dx$ and considering the first- and second-harmonic components of DW motion in Eq. (5), SMF voltage can be decomposed to first harmonic, $V_{\mathrm{SMF}}^{\omega}$, and second harmonic, $V_{\mathrm{SMF}}^{2\omega}$, components as

$$\begin{aligned}V_{\mathrm{SMF}}^{\omega}(t) &= V^{\omega}\sin[\omega t-\psi],\\ V_{\mathrm{SMF}}^{2\omega}(t) &= V^{2\omega}\sin[2\omega t-\xi],\end{aligned} \tag{14}$$

where the voltage amplitudes V^{ω} and $V^{2\omega}$ and the first-harmonic voltage phase ψ are given by

$$V^{\omega} = \frac{\hbar P\omega}{e\Delta}\sqrt{\beta^2A_\omega^2+\Delta^2\phi_\omega^2+2\beta\Delta A_\omega\phi_\omega\cos[\rho+\eta]},$$
$$\tan\psi = \frac{\beta A_\omega\sin[\delta-\rho]-\Delta\phi_\omega\sin[\delta+\eta]}{\beta A_\omega\cos[\delta-\rho]+\Delta\phi_\omega\cos[\delta+\eta]}, \tag{15}$$

$$V^{2\omega} = \frac{2\hbar P\omega\beta}{e\Delta}A_{2\omega}. \tag{16}$$

III. RESULTS AND DISCUSSIONS

A. DW dynamics

Implementing the realistic geometric and material parameters introduced in Table I and the current density value of $J = 20\times10^{13}$ A/m^2 [13,15,23,49] into Eqs. (5)–(7), we plot the DW motion amplitudes and components. Figure 2(a) shows A_ω (blue line) and $A_{2\omega}$ (red line) as functions of the applied current frequency, ω. There is a resonance peak in both the first- and second-harmonic amplitudes of 390 and 30 nm, respectively. The inset shows the second-harmonic amplitude separately for clarity. The resonance frequencies for first- and second-harmonic motion are current independent and for used material parameters they are obtained as $\omega_{r,1} = 59.9$ GHz and $\omega_{r,2} = 29.4$ GHz, respectively. It is obvious that the second-harmonic component of DW motion and its related effects are significant at second-harmonic resonance frequency, $\omega_{r,2}$. Therefore, we used $\omega = \omega_{r,2}$ to perform all other calculations hereafter. Figure 2(b) shows the time dependence of the

TABLE I. Realistic material parameters and geometry dimensions for numerical calculations [13,15,23,49].

	Symbol	Value	Unit
Saturation magnetization of FM	M_s	0.5	T
Exchange stiffness coefficient	A_{ex}	3.37×10^{-11}	J/m
Perpendicular anisotropy constants	K_u	1.5×10^5	J/m^3
Gilbert damping constant	α	0.02	
Nonadiabaticity of STT	β	0.05	
Restoring force constant	k	1.25×10^6	T^2/m
Conductivity of FM (NM)	σ_F (σ_N)	1.5×10^7 (1.89×10^7)	s/m
Spin polarization in the FM	P	0.5	
Spin Hall angle	θ_{SH}	0.15	
Domain wall width	Δ	15	nm
Thickness of FM (NM)	t_F (t_N)	0.6 (2)	nm
Applied current density	J	$(5-20)\times10^{13}$	A/m^2
Width of bilayer wire	w	5	nm
Half-length of bilayer wire	L	10×10^{-6}	m

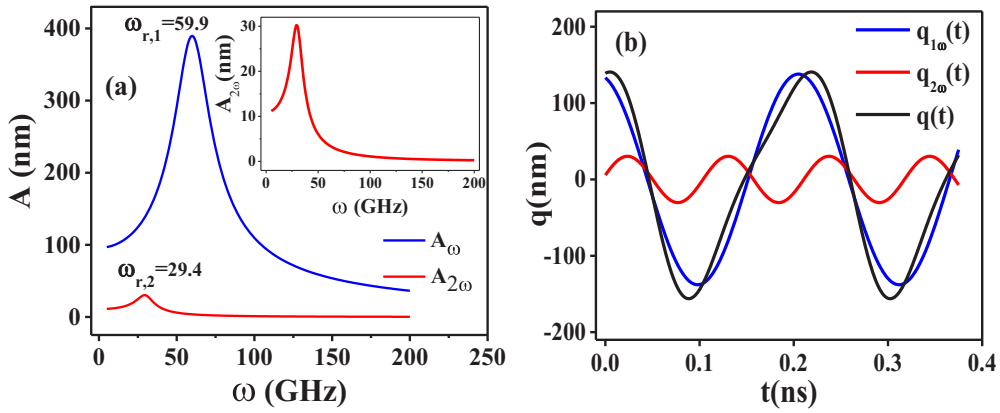

FIG. 2. (a) Frequency dependence of first-harmonic (A_ω) and second-harmonic ($A_{2\omega}$) amplitudes, respectively. The inset shows the second-harmonic motion amplitude separately. (b) Time dependence of first harmonic ($q_{1\omega}$), second harmonic ($q_{2\omega}$), and total (q) DW motion at second-harmonic resonance frequency, respectively. Applied current density is 20×10^{13} A/m^2.

first- (blue line) and second- (red line) harmonic components and the total (black line) DW motion, respectively.

B. SMF voltages

Using Eqs. (15) and (16) and the material parameters in Table I we obtain the current dependence of the first- and second-harmonic SMF voltage amplitudes at $\omega_{r,2}$ which are shown in Figs. 3(a) and 3(b), respectively. As mentioned earlier, A_ω and ϕ_ω linearly depend on the applied current, J, hence the first-harmonic voltage amplitude, V^ω, also depends linearly on J; whereas, the second-harmonic voltage amplitude, $V^{2\omega}$, quadratically grows with J due to the quadratic dependence of $A_{2\omega}$ on J.

C. Field-free spin Hall angle measurement based on electrical detection of second-harmonic DW resonance

Based on our results, we propose a field-free practical experimental method to measure the effective spin Hall angle for a bilayer FM/NM structure based on electrical detection of the current-driven second-harmonic DW resonance. In this technique, one can apply an ac current with constant amplitude to a bilayer strip of FM/NM structure and sweep the frequency and simultaneously probe the SMF second-harmonic voltage along the wire to find second-harmonic resonance frequency, $\omega_{r,2}$. Then, by fixing the frequency to second-harmonic resonance frequency and sweeping the current amplitude, one thus measures the current-dependent second-harmonic voltage. Fitting the result with Eq. (16), and using the appropriate material parameters, the effective spin Hall angle $\theta_{\rm SH}$ can be determined. This could be a powerful field-free and all-electrical method to measure spin Hall angle for FM/NM structures in comparison with any existing field required techniques such as C-FMR spectrometry [28,29], SP [30], ST-FMR [31,32], and hybrid phase-resolved OE-FMR [33]. All of these FMR-based techniques require large magnetic fields of the order of a few Teslas to saturate the FM layer and provide the FMR conditions. Along with this, the DW velocity measurement based techniques require a complicated measurement setup such as magneto-optical Kerr microscopy [34,35]. Therefore, our proposed technique represents the advantages of both field-free and simple all-electrical measurements. In addition, second-harmonic generation in FM/NM structures, by a DW or a noncollinear magnetization texture in general, could be useful in designing DW-based spin-torque signal generators and resonators.

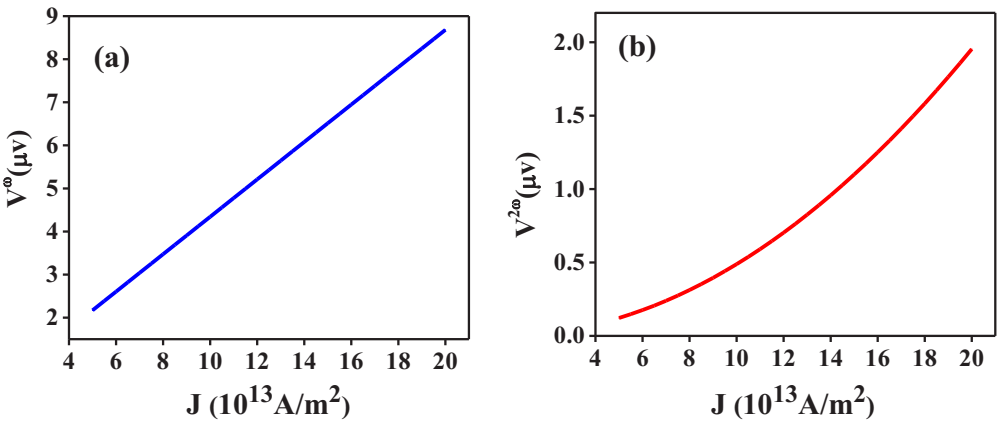

FIG. 3. Applied current density dependence of (a) first-harmonic (V^ω) and (b) second-harmonic ($V^{2\omega}$) SMF voltage amplitudes at second-harmonic resonance frequency.

IV. CONCLUSIONS

Using the real material parameters and reasonable current densities, we predict a second-harmonic DW resonance in FM/NM bilayer nanowires originating from ac SOT exerted on a FM layer. The longitudinal SMF-induced second-harmonic voltage is calculated in the range of $0.15-2\,\mu$V, which is measurable in laboratories. In addition, we introduced a field-free all-electrical method to obtain an effective spin Hall angle for FM/NM bilayer structures based on current-induced second-harmonic DW resonance. Furthermore, our results can help to efficiently design DW-based spin-torque signal generators and resonators.

ACKNOWLEDGMENTS

We acknowledge support from the Iran Science Elites Federation (ISEF).

M.R.H. and M.H. contributed equally to this work.

[1] M. Hayashi, L. Thomas, R. Moriya, C. Rettner, and S. S. P. Parkin, Science **320**, 209 (2008).
[2] D. A. Allwood, G. Xiong, C. C. Faulkner, D. Atkinson, D. Petit, and R. P. Cowburn, Science **309**, 1688 (2005).
[3] S. S. P. Parkin, M. Hayashi, and L. Thomas, Science **320**, 190 (2008).
[4] M. Ramu, I. Purnama, S. Goolaup, M. Chandra Sekhar, and W. S. Lew, J. Appl. Phys. **115**, 243908 (2014).
[5] S. Zhang and Z. Li, Phys. Rev. Lett. **93**, 127204 (2004).
[6] G. Tatara and H. Kohno, Phys. Rev. Lett. **92**, 086601 (2004).
[7] A. Thiaville, Y. Nakatani, J. Miltat, and Y. Suzuki, Europhys. Lett. **69**, 990 (2005).
[8] G. S. D. Beach, M. Tsoi, and J. L. Erskine, J. Magn. Magn. Mater. **320**, 1272 (2008).
[9] M. Kläui, P.-O. Jubert, R. Allenspach, A. Bischof, J. A. C. Bland, G. Faini, U. Rüdiger, C. A. F. Vaz, L. Vila, and C. Vouille, Phys. Rev. Lett. **95**, 026601 (2005).
[10] Z. Li and S. Zhang, Phys. Rev. B **70**, 024417 (2004).
[11] J. Sinova, S. O. Valenzuela, J. Wunderlich, C. H. Back, and T. Jungwirth, Rev. Mod. Phys. **87**, 1213 (2015).
[12] P. P. J. Haazen, E. Murè, J. H. Franken, R. Lavrijsen, H. J. M. Swagten, and B. Koopmans, Nat. Mater. **12**, 299 (2013).
[13] S. Emori, U. Bauer, S.-M. Ahn, E. Martinez, and G. S. D. Beach, Nat. Mater. **12**, 611 (2013).
[14] A. V. Khvalkovskiy, V. Cros, D. Apalkov, V. Nikitin, M. Krounbi, K. A. Zvezdin, A. Anane, J. Grollier, and A. Fert, Phys. Rev. B **87**, 020402 (2013).
[15] S.-M. Seo, K.-W. Kim, J. Ryu, H.-W. Lee, and K.-J. Lee, Appl. Phys. Lett. **101**, 022405 (2012).
[16] E. Martinez, S. Emori, and G. S. D. Beach, Appl. Phys. Lett. **103**, 072406 (2013).
[17] J. Ryu, K.-J. Lee, and H.-W. Lee, Appl. Phys. Lett. **102**, 172404 (2013).
[18] E. Saitoh, H. Miyajima, and T. Yamaoka, Nature (London) **432**, 203 (2004).
[19] G. Tatara, E. Saitoh, M. Ichimura, and H. Kohno, Appl. Phys. Lett. **86**, 232504 (2005).
[20] E. Martinez, L. Lopez-Diaz, O. Alejos, and L. Torres, Phys. Rev. B **77**, 144417 (2008).
[21] S. Lepadatu, O. Wessely, A. Vanhaverbeke, R. Allenspach, A. Potenza, H. Marchetto, T. R. Charlton, S. Langridge, S. S. Dhesi, and C. H. Marrows, Phys. Rev. B **81**, 060402 (2010).
[22] A. Bisig, L. Heyne, O. Boulle, and M. Kläui, Appl. Phys. Lett. **95**, 162504 (2009).
[23] P.-B. He, X. C. Xie, and W. M. Liu, Phys. Rev. B **72**, 172411 (2005).
[24] Y. K. Kato, R. C. Myers, A. C. Gossard, and D. D. Awschalom, Science **306**, 1910 (2004).
[25] J. Wunderlich, B. Kaestner, J. Sinova, and T. Jungwirth, Phys. Rev. Lett. **94**, 047204 (2005).
[26] E. Saitoh, M. Ueda, H. Miyajima, and G. Tatara, Appl. Phys. Lett. **88**, 182509 (2006).
[27] T. Kimura, Y. Otani, T. Sato, S. Takahashi, and S. Maekawa, Phys. Rev. Lett. **98**, 156601 (2007).
[28] K. Ando, S. Takahashi, K. Harii, K. Sasage, J. Ieda, S. Maekawa, and E. Saitoh, Phys. Rev. Lett. **101**, 036601 (2008).
[29] S. Emori, T. Nan, T. M. Oxholm, C. T. Boone, J. G. Jones, B. M. Howe, G. J. Brown, D. E. Budil, and N. X. Sun, Appl. Phys. Lett. **106**, 022406 (2015).
[30] O. Mosendz, J. E. Pearson, F. Y. Fradin, G. E. W. Bauer, S. D. Bader, and A. Hoffmann, Phys. Rev. Lett. **104**, 046601 (2010).
[31] L. Liu, T. Moriyama, D. C. Ralph, and R. A. Buhrman, Phys. Rev. Lett. **106**, 036601 (2011).
[32] T. Chiba, G. E. W. Bauer, and S. Takahashi, Phys. Rev. Appl. **2**, 034003 (2014).
[33] A. Capua, T. Wang, S.-H. Yang, C. Rettner, T. Phung, and S. S. P. Parkin, Phys. Rev. B **95**, 064401 (2017).
[34] K.-S. Ryu, L. Thomas, S.-H. Yang, and S. Parkin, Nat. Nanotechnol. **8**, 527 (2013).
[35] K.-S. Ryu, S.-H. Yang, L. Thomas, and S. S. P. Parkin, Nat. Commun. **5**, 3910 (2014).
[36] K.-W. Kim, J.-H. Moon, K.-J. Lee, and H.-W. Lee, Phys. Rev. Lett. **108**, 217202 (2012).
[37] K. Garello, I. M. Miron, C. O. Avci, F. Freimuth, Y. Mokrousov, S. Blügel, S. Auffret, O. Boulle, G. Gaudin, and P. Gambardella, Nat. Nanotechnol. **8**, 587 (2013).
[38] M. Hayashi, J. Kim, M. Yamanouchi, and H. Ohno, Phys. Rev. B **89**, 144425 (2014).
[39] C. O. Avci, A. Quindeau, C.-F. Pai, M. Mann, L. Caretta, A. S. Tang, M. C. Onbasli, C. A. Ross, and G. S. D. Beach, Nat. Mater. **16**, 309 (2016).
[40] C. O. Avci, K. Garello, M. Gabureac, A. Ghosh, A. Fuhrer, S. F. Alvarado, and P. Gambardella, Phys. Rev. B **90**, 224427 (2014).
[41] C. O. Avci, K. Garello, C. Nistor, S. Godey, B. Ballesteros, A. Mugarza, A. Barla, M. Valvidares, E. Pellegrin, A. Ghosh, I. M. Miron, O. Boulle, S. Auffret, G. Gaudin, and P. Gambardella, Phys. Rev. B **89**, 214419 (2014).
[42] S. Luo, Y. Zhang, M. Shen, J. Ou-Yang, B. Yan, X. Yang, S. Chen, B. Zhu, and L. You, Appl. Phys. Lett. **110**, 112402 (2017).

[43] N. L. Schryer and L. R. Walker, J. Appl. Phys. **45**, 5406 (1974).
[44] E. Martinez, L. Lopez-Diaz, O. Alejos, L. Torres, and C. Tristan, Phys. Rev. Lett. **98**, 267202 (2007).
[45] R. A. Duine, Phys. Rev. B **77**, 014409 (2008).
[46] R. A. Duine, Phys. Rev. B **79**, 014407 (2009).
[47] Y. Tserkovnyak and M. Mecklenburg, Phys. Rev. B **77**, 134407 (2008).
[48] R. Cheng, J.-G. Zhu, and D. Xiao, J. Phys. D. Appl. Phys. **49**, 434001 (2016).
[49] Although DW dynamics highly depends on the relative values of α and β [46], we fixed them at given values and do not concentrate on their effects in this work.